11. J. Broadhead, in "Power Sources 4," D. H. Collins, Editor, Oriole Press, Newcastle upon Tyne, England (1973); U.S. Pat. 3,791,867.
12. R. D. Rauh, K. M. Abraham, G. F. Pearson, J. K. Suprenant, and S. B. Bummer, *This Journal*, **126**, 523 (1979).
13. Freeman, Oklahoma State Univ. Research Foundation Report No. 60 (1962).

Semiconductor Electrodes

XXXVI. Characteristics of n-$MoSe_2$, n- and p-WSe_2 Electrodes in Aqueous Solution

Fu-Ren F. Fan* and Allen J. Bard*

Department of Chemistry, The University of Texas at Austin, Austin, Texas 78712

ABSTRACT

Capacitance and voltammetric measurements were employed to investigate the electrochemical and photoelectrochemical (PEC) behavior of n-WSe_2, p-WSe_2, and n-$MoSe_2$ single crystal electrodes in aqueous solutions containing various redox couples (Br^-/Br_2, I^-/I_3^-, $Fe(CN)_6^{4-}/Fe(CN)_6^{3-}$, Fe^{2+}/Fe^{3+}, $HV^{+\cdot}/HV^{2+}$, and $MV^{+\cdot}/MV^{2+}$, where HV is heptyl viologen and MV is methyl viologen). In supporting electrolyte (0.5M Na_2SO_4), the conduction bandedges of $MoSe_2$ and WSe_2, determined from the capacitance measurement, are at -0.14 and -0.44V *vs.* SCE, respectively, and the valence bandedge of WSe_2 is at 0.93V *vs.* SCE. A bandgap of 1.4 eV for WSe_2 was determined either from the photocurrent action spectrum or from the capacitance measurement. The specific effects of iodide on the capacitance and voltammetric behavior of layer-type compounds are compared. The characteristics of several PEC cells are also described.

The application of semiconductor electrode photoelectrochemical (PEC) cells (1) for the utilization of solar energy for the production of electricity or chemical species depends on the discovery of inexpensive and abundant materials with an energy gap which matches the solar spectrum and which are capable of stable operation. Thus there has been an active search for new semiconductor materials for PEC cells which meet these requirements.

Tributsch (2) introduced the concept of using layer-type electrodes (*e.g.*, MoS_2, $MoSe_2$, WSe_2) for such applications and a number of recent papers (3-8)[1] have described PEC cells based on these materials. These cells show quite good efficiencies and good stability in aqueous and acetonitrile solutions containing redox couples with reasonably positive redox potentials (*e.g.*, I^-/I_3^-). Wrighton and co-workers demonstrated that $MoSe_2$ and MoS_2 can even photo-oxidize chloride in highly concentrated aqueous LiCl solutions (3).

The behavior and efficiencies of these cells depend strongly on the nature of the electrode surface (4-8). A wide range of scatter in the electrochemical parameters (*e.g.*, flatband potential, V_{FB}) and the PEC behavior is reported from different laboratories. These different results are apparently due to the significant sample-to-sample variations in the morphology of crystals. For example, the presence of exposed edges in the van der Waals surface ($\perp$ C-axis) has been shown to lead to significant dark anodic currents at n-type electrodes and lower photocurrent efficiencies (4c, 8b).

In this report, we describe the voltammetric and impedance measurements of some carefully selected and well-behaved n-$MoSe_2$, n- and p-WSe_2 single crystals. Some physical properties, *e.g.*, V_{FB} and the bandgap, E_g, of WSe_2, obtained by different techniques are compared. The specific effect of iodide on the onset photopotentials of layer-type compounds is compared with V_{FB} obtained by capacitance measurements. We also discuss the performance of several solar cells composed of n-$MoSe_2$ and (halogen/halide) redox couples.

* Electrochemical Society Active Member.
Key words: capacitance, voltammetry, impedance, photoelectrochemical behavior, solar cells.
[1] A solar power conversion efficiency of 10.2% has been reported for a cell based on n-WSe_2 and I^-/I_3^- systems (5).

Experimental

The semiconductors used, n-$MoSe_2$, n- and p-WSe_2, were single crystals generously donated by Dr. Barry Miller and Dr. Frank DiSalvo, Bell Laboratories. The detailed procedures for selecting, mounting, cleaning, and etching the single crystals and preparing the ohmic contacts are similar to those previously reported (4). The electrodes studied here showed mirror-like surfaces with no obvious edges and pits on the surfaces when examined at a magnification of 100×. They produced negligibly small dark oxidation currents ($< 1\ \mu A\ cm^{-2}$) in 0.5M Na_2SO_4 between -0.5 and 1V *vs.* SCE. Typically, the electrode areas of the semiconductors were 0.03-0.2 cm^2. If not otherwise mentioned, the exposed surface is the van der Waals surface ($\perp$ C-axis).

A conventional three-electrode, single-compartment cell was used for all experiments. The electrochemical cell (volume $\sim$ 25 ml) contained Pt disk and semiconductor working electrodes and was fitted with a flat Pyrex window for illumination of the semiconductor electrode. A platinum foil ($\sim$ 40 cm^2) was used as the counterelectrode in the voltammetric and impedance measurements. An aqueous saturated calomel electrode (SCE) was used as the reference electrode.

The voltammetric experiments and the solar cell measurements were performed with the same apparatus and procedures as reported previously (4). The light source used in the study of the PEC effect was an Oriel Corporation (Stamford, Connecticut) 450W Xe lamp. Experiments designed for specific wavelengths employed an Oriel 7240 grating monochromator with a 20 nm bandpass. A red filter (590 nm cut-on) was used with the Xe lamp. The radiant intensity was measured with an EG & G (Salem, Massachusetts) Model

550 Radiometer/Photometer. Neutral density filters were used to vary the intensity of the light.

All impedance measurements were carried out with an aqueous 0.5M Na_2SO_4 solution, if not otherwise mentioned. The electrical circuit allowed the application of a variable potential at the semiconductor electrode with respect to the reference electrode. The impedance was measured between this working electrode and a large ($\sim$ 40 cm^2) counterelectrode. The applied potential was controlled potentiostatically, and the capacitance was measured as the 90° quadrature signal from a lock-in amplifier (Princeton Applied Research, Model HR-8) with excitation by an external a-c generator via the potentiostat. The amplitude of the sinusoidal wave superimposed on the d-c bias potential was $\sim$ 5 mV. The measured capacitances were calibrated by replacing the electrochemical cell by a set of standard capacitors. The quantity measured was the equivalent series capacitance, C, since the dissipation factor ωRC, where ω is the angular frequency and R is equivalent series resistance, was much smaller than unity for all systems studied here, as shown in the results below. The measured impedance values were not changed when the counterelectrode was partially lifted out of the solution; thus the counterelectrode did not contribute significantly to the reported capacitances. All impedance measurements were performed in the dark.

Reagent grade chemicals were used without further purification. All solutions were prepared from triply distilled water and were deoxygenated for at least 30 min with purified nitrogen before each experiment. All experiments were carried out with the solution under a nitrogen atmosphere.

Results

Impedance measurements.—The capacitance of an electrode as a function of frequency and potential was a useful indicator of the electrode quality. The n-$MoSe_2$ and n-WSe_2 electrodes were subjected to impedance measurements in supporting electrolyte solutions, if not otherwise mentioned, at d-c bias potentials where the residual currents were negligibly small (< 1 μA cm^{-2}). Thus the measured value of C is the equivalent differential capacitance of the interface, with no faradaic contribution. If the presence of the oxidized form of a redox couple was required, its concentration was kept as low as possible to prevent substantial reduction current, which might distort the Mott-Schottky plots.

The value of the flatband potential, V_{FB}, was determined from the intercept of the plot of $1/C^2$ *vs.* potential according to the Mott-Schottky equation (9)

$$\left(\frac{1}{C}\right)^2 = \frac{2}{\epsilon\epsilon_0 e_0 n}\left(|V - V_{fb}| - \frac{kT}{e_0}\right) \qquad [1]$$

In this equation ϵ is the dielectric constant of the semiconductor, ϵ_0 is the permittivity of free space, n is the donor density, n_D, for n-type and the acceptor density, n_A, for p-type semiconductors, e_0 is the absolute value of the charge of the electron, T is the absolute temperature, and k is the Boltzmann constant.

n-$MoSe_2$.—As shown in Fig. 1a, at frequencies between 1 and 10 kHz, a linear C^{-2} *vs.* V relationship was observed over a considerable potential range. Since the capacitance at these potentials is frequency independent, the intercept of the Mott-Schottky plot gives the flatband potential after correction for the thermal term in Eq. [1] and the potential drop across the Helmholtz double layer (*i.e.*, for the contribution of capacitance of the Helmholtz layer). The flatband potential of this n-$MoSe_2$ electrode was $\sim$0.0V *vs.* SCE at pH 4.5.

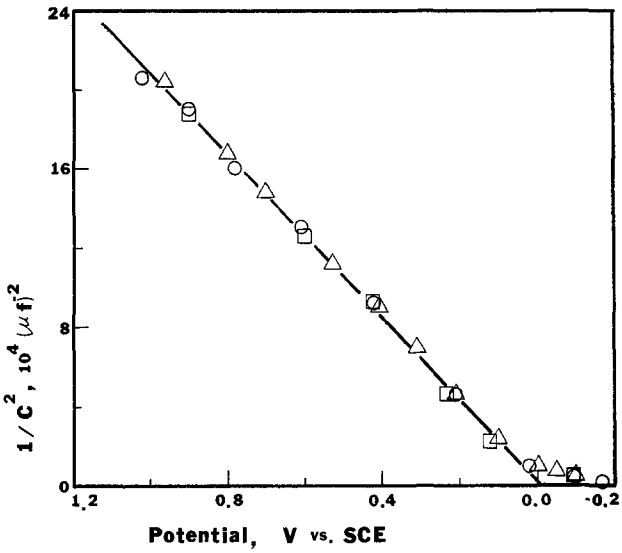

Fig. 1a. C^{-2} *vs.* V at different frequencies for n-$MoSe_2$ electrode in aqueous solution of 0.5M Na_2SO_4 at pH 4.5: (□) 1 kHz, (○) 3 kHz, (△) 10 kHz. Electrode area, 0.030 cm^2.

If we take the dielectric constant perpendicular to the C-axis, $\epsilon_\perp$, as 6.8 (10),[2] the slope of the Mott-Schottky plot yields $n_D \sim 1.2 \times 10^{17}$ cm^{-3}. With this value of the donor density of the $MoSe_2$ single crystal, the location of conduction bandedge, E_c, was calculated from Eq. [2] (9), assuming that the donor impurities are completely ionized. Since $N_c >> n_D$ (see below)

$$n_D = N_c \exp\left[-(E_c - E_F)/kT\right] \qquad [2]$$

in which E_F is the Fermi energy and N_c is the density of the effective states in the conduction band, which is given by

$$N_c = 2\left(\frac{2\pi M_e^* kT}{h^2}\right)^{3/2} \qquad [3]$$

where h is the Planck constant and M_e^* is the effective mass of electrons in the conduction band. With the assumption $M_e^* \approx M_0$ (11),[3] in which M_0 is the mass of a free electron, N_c was estimated to be $\sim 2.5 \times 10^{19}$ cm^{-3}. Thus, E_c was $\sim$ 0.14 eV above the V_{FB} Fermi level energy, *i.e.*, the conduction bandedge is located at a potential $\sim$ — 0.14V *vs.* SCE.

The frequency independence of the capacitance implies that no oxide layer was on the surface of $MoSe_2$. The presence of an oxide layer often leads to frequency dispersion in the measured capacitance values because of dielectric relaxation in this layer.

As shown in Fig. 1b, the flatband potential of the n-$MoSe_2$ electrode was independent of pH, at least in the range studied (0-8). This finding further confirms the absence of an oxide layer on the electrode surface.

The flatband potential of the n-$MoSe_2$ electrode shifted to a more negative potential when iodide was present in the solution (Fig. 2a). Moreover, addition of a small amount of triiodide (0.25 mmole) shifted V_{FB} to an even more negative potential. However, bromide had no effect on V_{FB} (Fig. 2b). These results parallel those obtained by the voltammetric measurements which are described later. We can also estimate the resistivity, ρ, of this n-$MoSe_2$ electrode from the mobility, μ_e, of electrons and the free electron density, n_e, based on Eq. [4]

$$\rho \cong 1/(e_0 n_e \mu_e) \qquad [4]$$

Here we neglect the contribution from the minority

[2] The $\epsilon_\perp$ value of $MoSe_2$ was assumed close to that of MoS_2. The $\epsilon_\perp$ of MoS_2 has been reported by Evans *et al.* (10).

[3] Here we assume that electrons in $MoSe_2$ have similar effective mass to that in WSe_2 (11).

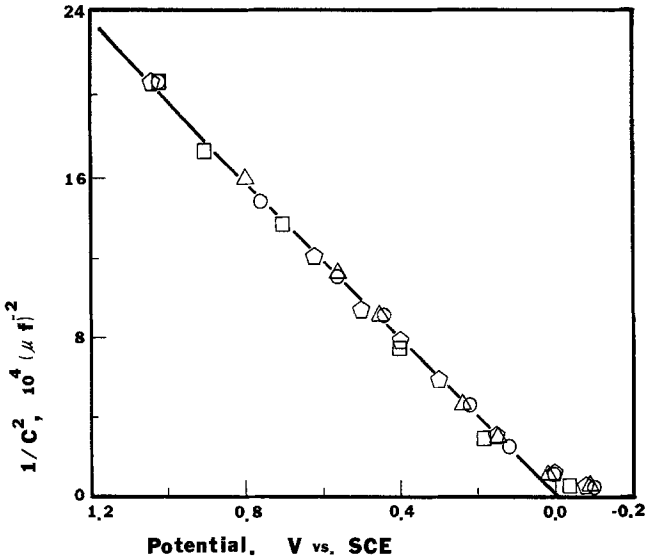

Fig. 1b. C^{-2} *vs.* V at different pH for n-$MoSe_2$ electrode in aqueous solution of 0.5M Na_2SO_4 at 2 kHz; (□) pH 0.5, (○) pH 2.5, (△) pH 4.5, (⬠) pH 8.0.

charge carriers. With $\mu_e = 10 \sim 50$ cm^2 V^{-1} sec^{-1} (12) and the assumption that the donors are completely ionized, ρ can be estimated to be $1 \sim 5$ Ω-cm.

n-WSe_2.—The general behavior for n-WSe_2 electrodes was similar to that of the n-$MoSe_2$ electrode described above. At frequencies between 0.2 and 2 kHz, a linear C^{-2} *vs.* V relationship was obtained over a considerable potential range and the capacitance was essentially frequency independent (see Fig. 3). Thus, V_{fb} of this n-WSe_2 electrode was ~ -0.32V *vs.* SCE. Assuming that $\epsilon_\perp \approx 10$ for WSe_2 (13),[4] we estimate a donor density of this electrode of $\sim 2.0 \times 10^{17}$ cm^{-3}. According to Hicks (11), $M_e^* \approx M_h^* \approx M_o$; hence N_c was $\sim 2.5 \times 10^{19}$ cm^{-3} and E_c was ~ 0.12 eV beyond the V_{FB} Fermi level energy. With $\mu e = 100 \sim 150$ cm^2 V^{-1} sec^{-1} for the n-WSe_2 single crystals (12), the resistivity of this n-WSe_2 is $0.1 \sim 0.2$ Ω-cm.

p-WSe_2.—As shown in Fig. 4a, p-WSe_2 electrodes show quite different capacitance-potential curves from their n-counterparts. With potentials positive of 0.05V *vs.* SCE, a linear C^{-2} *vs.* V relationship was observed at frequencies of 1-10 kHz (Fig. 5a). For potentials more negative than 0.05V *vs.* SCE, frequency dispersion of capacitance occurs. The capacitance at − 0.2V *vs.* SCE for p-WSe_2 follows a (frequency)$^{-2}$ dependence at frequencies > 2 kHz. The origin of this frequency dispersion is still not clear, but might involve the presence of interface states or the onset inversion coupled with a faradaic process. Further investigations are required to explain this behavior.

[4] An approximate value was taken here since the exact dielectric constant at the frequency range studied is unknown (13).

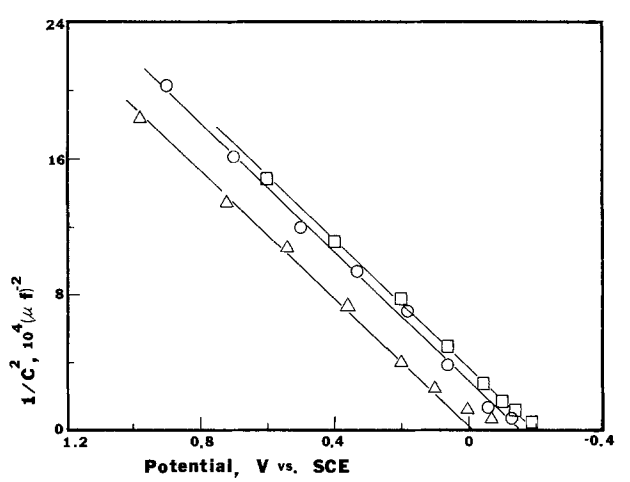

Fig. 2a. C^{-2} *vs.* V at 2 kHz for n-$MoSe_2$ electrode in aqueous solution of 0.5M Na_2SO_4 without containing iodide and triiodide (△), in the presence of 1.0M diodide (○), and in the presence of 1.0M iodide and 0.25 mmoles triiodide (□).

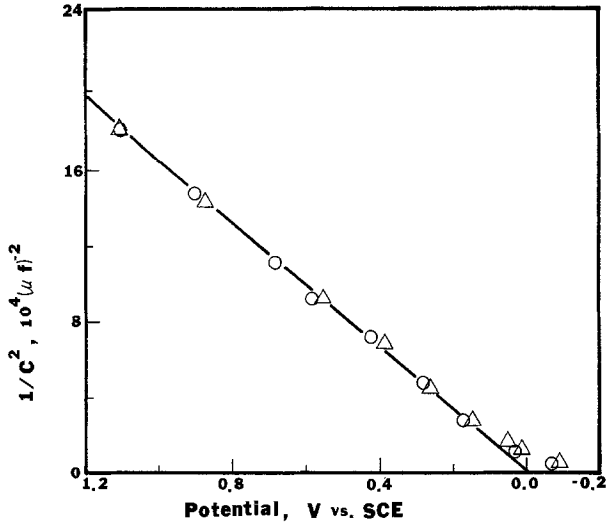

Fig. 2b. The effect of bromide on the Mott-Schottky plots on n-$MoSe_2$ in aqueous solution of 0.5M Na_2SO_4 at 2 kHz: (△) no bromide, (○) 1.0M bromide.

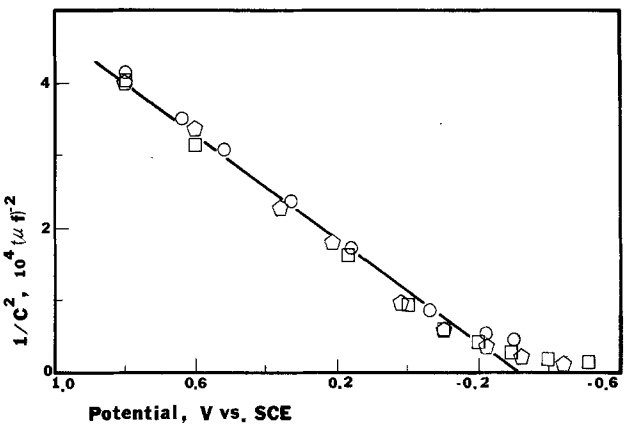

Fig. 3. The Mott-Schottky plots at different frequencies for n-WSe_2 electrode in aqueous solution of 0.5M Na_2SO_4 at pH 4.5: (⬠) 200 Hz, (□) 500 Hz, (○) 2 kHz. Electrode area, 0.049 cm^2.

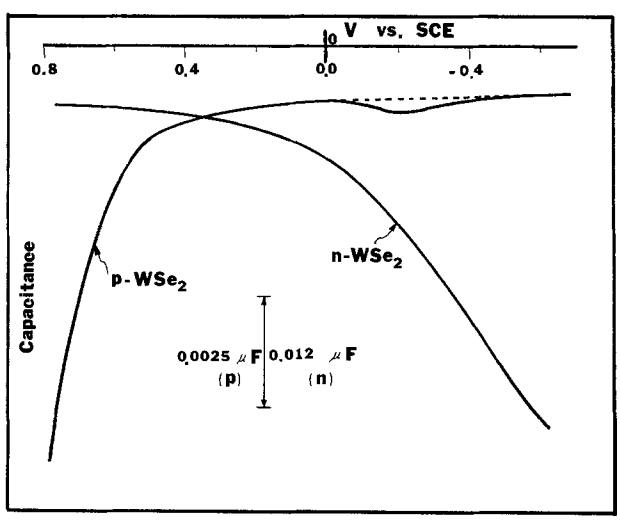

Fig. 4a. The capacitance-potential curves for n- and p-WSe_2 electrodes at 5 kHz in aqueous solution of 0.5M Na_2SO_4 at pH 4.5.

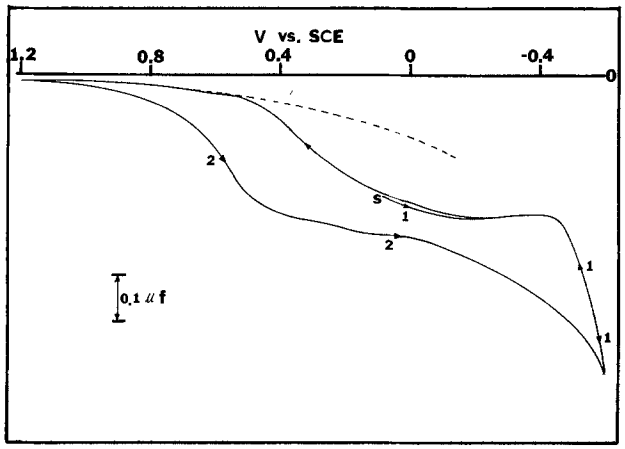

Fig. 4b. Capacitance *vs.* potential plot for n-WSe_2 electrode, type E. The potential was scanned beginning at point "s" at 5 mV/sec in the direction indicated by the arrows. $f = 200$ Hz. The dotted line indicates the expected capacitance for an electrode following the Mott-Schottky relation.

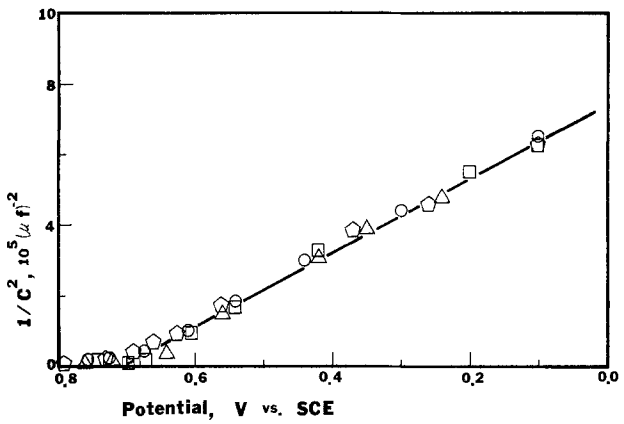

Fig. 5a. C^{-2} *vs.* *V* at different frequencies for p-WSe_2 electrode in aqueous solution of 0.5M Na_2SO_4 at *p*H 4.5: (△) 1 kHz, (◇) 2 kHz, (□) 5 kHz, (○) 10 kHz. Electrode area, 0.050 cm^2.

Since frequency dispersion is found only at potentials negative of 0.0V *vs.* SCE which is well negative of V_{FB}, it has essentially no effect on the Mott-Schottky plots as shown in Fig. 5a. V_{FB} of this p-WSe_2 electrode was thus ~ 0.72V *vs.* SCE. If $\epsilon \approx 10$ for WSe_2 (13), the acceptor density of this electrode can be estimated as $\sim 5 \times 10^{15}$ cm^{-3}. The density of effective states in the valence band of WSe_2, N_v, the energy of the valence bandedge, E_v, and the resistivity of this p-WSe_2 are shown in Table I. As found with n-$MoSe_2$, V_{FB} of p-WSe_2 is *p*H independent (Fig. 5b) in the *p*H range studied.

The capacitance-potential plots which correspond well to that expected of the semiconductor space charge capacitance (*e.g.*, well-behaved Mott-Schottky plots

Table I. Impurity densities, bandedges, effective densities of states in the conduction, and valence bands and resistivities of $MoSe_2$ and WSe_2 samples*

	n-$MoSe_2$	WSe_2
n (cm^{-3})	1.2×10^{17}	2.0×10^{17} (n) 5×10^{15} (p)
E_c (V *vs.* SCE)	−0.14	−0.44
E_v (V *vs.* SCE)	1.26	0.93
N_c (cm^{-3})	—	2.5×10^{19}
N_v (cm^{-3})	—	2.5×10^{19}
ρ (Ω-cm)	1 ~ 5	0.1 ~ 0.2 (n) 5 ~ 10 (p)

* In aqueous solution of 0.50M Na_2SO_4.

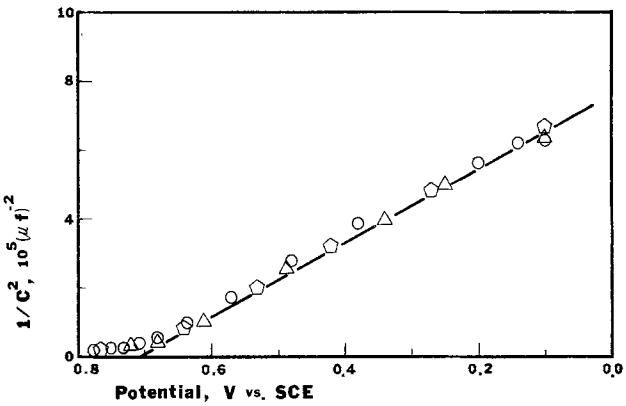

Fig. 5b. The *p*H effect on the Mott-Schottky plots at 5 kHz for p-WSe_2 electrode in aqueous solution of 0.5M Na_2SO_4: (○) *p*H 1, (△) *p*H 4.5, (◇) *p*H 8.

and frequency independence) found with edge-free electrode material (*e.g.*, Fig. 4a for n-WSe_2) can be contrasted with that found with material which contains some edges and discontinuities on the surfaces [designated "type E" in previous studies (4c)]. For type E n-WSe_2 electrodes, discontinuities are seen in the capacitance plots (Fig. 4b) as well as hysteresis effects and frequency dispersion. Thus capacitance plots are useful in distinguishing electrode material which produces low dark currents and efficient PEC cells from less efficient (type E) material.

Voltammetric behavior.—Electrochemical and PEC behavior of n- and p-WSe_2 electrodes have been reported previously (4). The following results mainly involve n-$MoSe_2$ electrodes. The voltammetric behavior of iodide at n-$MoSe_2$ and Pt is shown in Fig. 6. With or without I^- in the solution, in the dark a negligibly small background current was observed (curves a and b). Under illumination with slowly chopped red light (wavelength ≧ 590 nm), an anodic photocurrent commencing at 0.5V *vs.* SCE (curve c) was observed in the supporting electrolyte containing 0.50M H_2SO_4. No cathodic photocurrent was found, as expected for an n-type material. In the presence of 1.0M NaI, the onset photopotential, V_{on}, shifted to a much more negative potential, − 0.26V *vs.* SCE (curve d). The addition of iodine (0.10M) to the solution shifted V_{on} to slightly more negative potentials (~ −0.30V *vs.* SCE) (curve e). Note that the specific effects of iodide and triiodide on V_{on} parallel their effects on the V_{FB} determined from impedance measurements. The current-potential curves on Pt (curve f) and n-$MoSe_2$ in an I^-/I_3^- solution yield an "underpotential" for I^- photo-oxidation at n-$MoSe_2$ $V_{on} - V_{redox}$, of − 0.59V. This value agrees fairly well with the experimental open-circuit voltage, V_{oc}, of an n-$MoSe_2/I_2$, I^-/Pt PEC cell described below.

The voltammetric data and photopotentials of other redox couples on n-$MoSe_2$ electrodes are summarized in Table II. For redox couples with standard potentials, V^o, much more negative than V_{FB}, no photoeffect was observed. The V_{on} for the redox couples with $V_{FB} < V^o < 0.29$V *vs.* SCE (except for I^-/I_3^-) are nearly independent of the redox couples and are close to V_{FB} (~ 0.0V *vs.* SCE). For redox couples with 0.50V < V^o < 1.0V *vs.* SCE, V_{on} depended on the particular species and varied from ~ 0.25V for Br^- to ~ 0.50V for background oxidation. The photo-oxidation of compounds with V^o more positive than for water oxidation is uncertain because of the background photoreaction. It is interesting to compare the reduction of various oxidants on n-$MoSe_2$ electrodes in the dark. As shown in Fig. 7, reduction of bromine (curve a) and Fe^{3+} (curve b) occurs at potentials negative of 0.5V *vs.* SCE

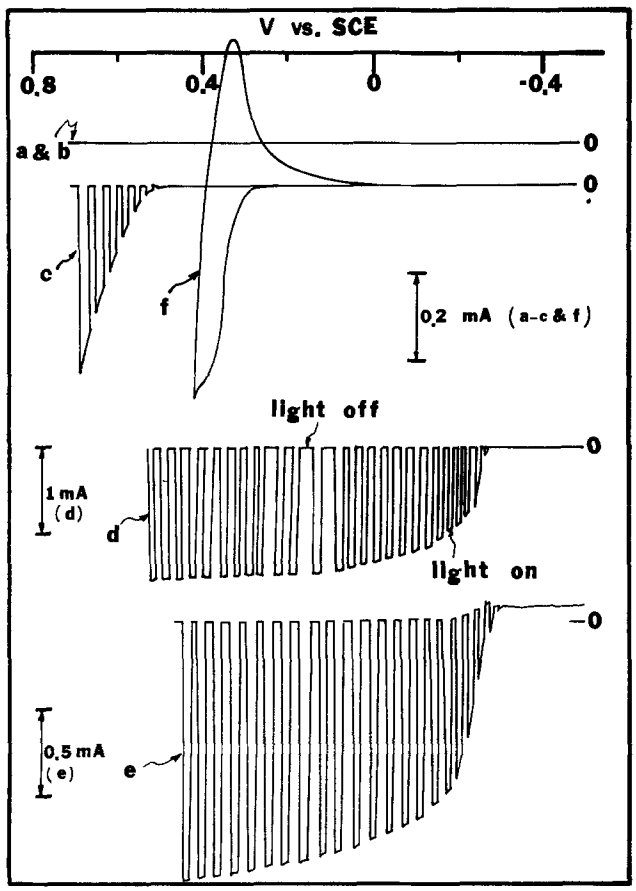

Fig. 6. Voltammetric curves of n-$MoSe_2$ and Pt in 0.5M Na_2SO_4 and 0.5M H_2SO_4. Scan rate, 10 mV/sec. Light source, 450W Xe lamp with a 590 nm cut-on filter. (a) Dark cyclic voltammogram on n-$MoSe_2$. (b) Dark cyclic voltammogram on n-$MoSe_2$. Solution contained 1.0M NaI. (c) Voltammetric curve under illumination by chopped red light on n-$MoSe_2$. No iodide or iodine in solution. (d) Current-potential curve under illumination by chopped red light on n-$MoSe_2$. Solution contained 1.0M NaI. (e) Same conditions as in (d) but solution contained 1.0M NaI and 0.10M iodine. (f) Cyclic voltammogram on Pt. Solution contained 0.10M NaI. Initial potential at −0.10V vs. SCE.

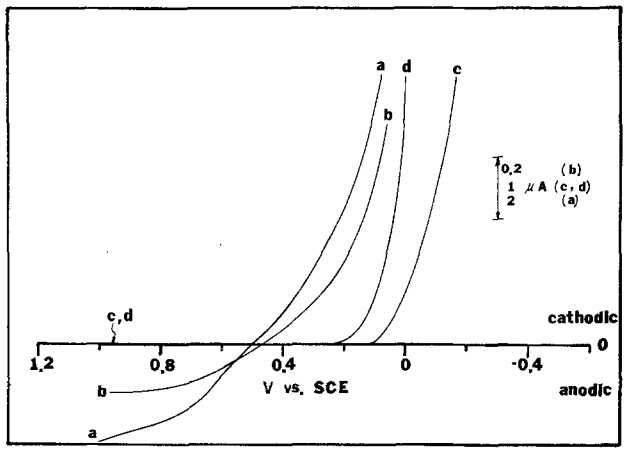

Fig. 7. Voltammetric curves in the dark on n-$MoSe_2$ electrode in 0.50M Na_2SO_4. Scan rate, 10 mV/sec. (a) Solution contained 1.0M NaBr and 0.02M bromine. (b) Solution contained 0.10M Fe^{2+}, 0.02M Fe^{3+}, and 0.50M H_2SO_4. (c) Solution contained 1.0M NaI and 0.10M iodine. (d) Solution contained 0.1M $Fe(CN)_6^{4-}$ and 0.1M $Fe(CN)_6^{3-}$.

(well positive of V_{FB}). However, iodine reduction occurs only at potentials well negative of 0.1V *vs.* SCE (curve c). The reduction of ferricyanide (curve d) occurs at a potential ~ 0.25V *vs.* SCE. Under irradiation these significant cathodic currents would constitute a back-reaction of a photogenerated oxidant which can affect the performance of the solar cells, as described below.

Photovoltaic cell measurements.—Regenerative semiconductor/liquid junction solar cells were fabricated by immersing the semiconductor electrode and a suitable counterelectrode in an aqueous solution containing the appropriate redox couple.

The n-$MoSe_2$/iodide, triiodide/Pt system.—Photovoltaic cells were set up with an n-$MoSe_2$ photoanode and a platinum foil cathode immersed in a solution containing 1.0M I^-, 0.025M I_3^-, and 1.0M H^+. The action spectrum of the short-circuit photocurrent, i_{ss}, is shown in Fig. 8. The bandgap of WSe_2 and $MoSe_2$ can be determined from the $(\eta h\nu)^2$ *vs.* $h\nu$ plot (for a direct transition) or the $(\eta h\nu)^{1/2}$ *vs.* $h\nu$ plot (for an indirect transition) near the bandedge region (14). η here is the quantum efficiency (proportional to i_{ss}) and $h\nu$ is the photon energy. As shown in Fig. 9, both $(\eta h\nu)^2$ *vs.* $h\nu$ and $(\eta h\nu)^{1/2}$ *vs.* $h\nu$ plots give fairly good straight lines. The nature of the fundamental optical transition is thus ambiguous as simply determined from the action spectrum. However, the determination of E_g from the capacitance measurements, as discussed later, is helpful in deciding on the value of E_g.

The *i-V* characteristics of this cell under irradiation, shown in Fig. 10, yields a fill factor of 0.53. The light intensity dependence of the open-circuit photovoltage and the short-circuit photocurrent of the cell is shown in Fig. 11. Irradiation of the n-$MoSe_2$ crystal with the full visible (longer than 590 nm and infrared filtered) output (150 mW/cm²) from a 450W Xe lamp focused onto the photoelectrode surface yielded a constant i_{ss} ~ 50 mA/cm² and an open-circuit photovoltage ~0.59V. The photocurrent and photovoltage were essentially the same and the electrode surface showed no apparent change during the experimental period (~8 hr).

Table II. Voltammetric data, onset photopotential* and underpotential at n-$MoSe_2$

Redox couple	V° (V *vs.* SCE)**	V_{on} (V *vs.* SCE)	Experimental underpotential, $\Delta V = V_{on} - V^\circ$ (V)	Theoretical underpotential,*** $\Delta V' = V_{FB} - V^\circ$ (V)
Cl^-/Cl_2 (pH = 0)	1.12	—	—	−1.12
H_2O/O_2 (pH = 0)	0.99	0.50	−0.49	−0.99
Br^-/Br_2 (pH = 0)	0.82	0.25	−0.57	−0.82
Fe(II)/Fe(III) (1*N* H_2SO_4)	0.53	0.30	−0.23	−0.53
I^-/I_2 (pH = 0)	0.29	−0.30	−0.59	−0.59
$Fe(CN)_6^{4-}/Fe(CN)_6^{3-}$ (pH = 6)	0.22	0.02	−0.20	−0.22
Fe(II)-EDTA/Fe(III)-EDTA (pH = 5)	−0.15	0.0	No	No
HV^+/HV^{2+}† (pH = 5)	−0.48	No photoeffect	—	—
MV^+/MV^{2+}‡ (pH = 2.5)	−0.66	No photoeffect	—	—

* The onset photopotential V_{on} here is defined as the potential at which 1% of the limiting or maximal photocurrent is observed.
** V° = standard potential.
*** V_{FB} is based on that obtained from the impedance measurement. It is −0.3V *vs.* SCE for I^-/I_3^- and 0V for other redox couples.
† HV = heptyl viologen (1,1'-diheptyl-4,4' bipyridyl).
‡ MV = methyl viologen (1,1'-dimethyl-4,4'-bipyridyl).

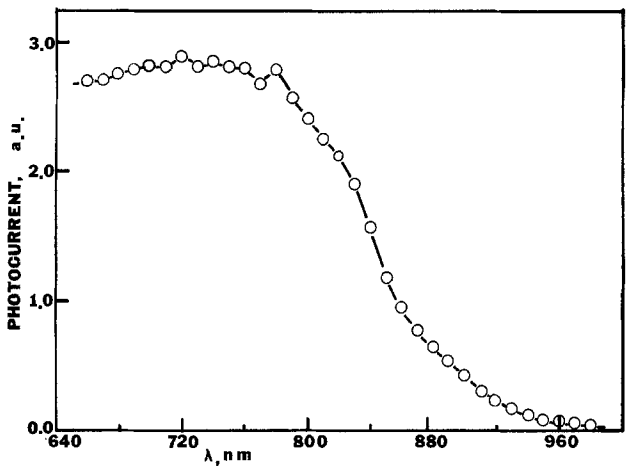

Fig. 8. Action spectrum of the short-circuit photocurrent for an n-$MoSe_2$/1.0M NaI, 0.05M I/Pt solar cell. The spectrum has been corrected for the solution absorbance.

The n-$MoSe_2$/bromide, bromine/Pt system.—When a solution containing 1.0M Br^-, 0.02M Br_2, and 1.0M H^+ was used as the electrolyte, a lower open-circuit photovoltage (0.52V), and a lower fill factor (0.25) were found (Fig. 10) (15).[5] However, the short-circuit photocurrent was higher (~60 mA/cm²) under the same intensity irradiation. This difference is probably attributable to the lower light absorbance by the Br^-,

[5] Solar cells with higher fill factors but lower open-circuit voltages have been reported by Ang *et al.* (15).

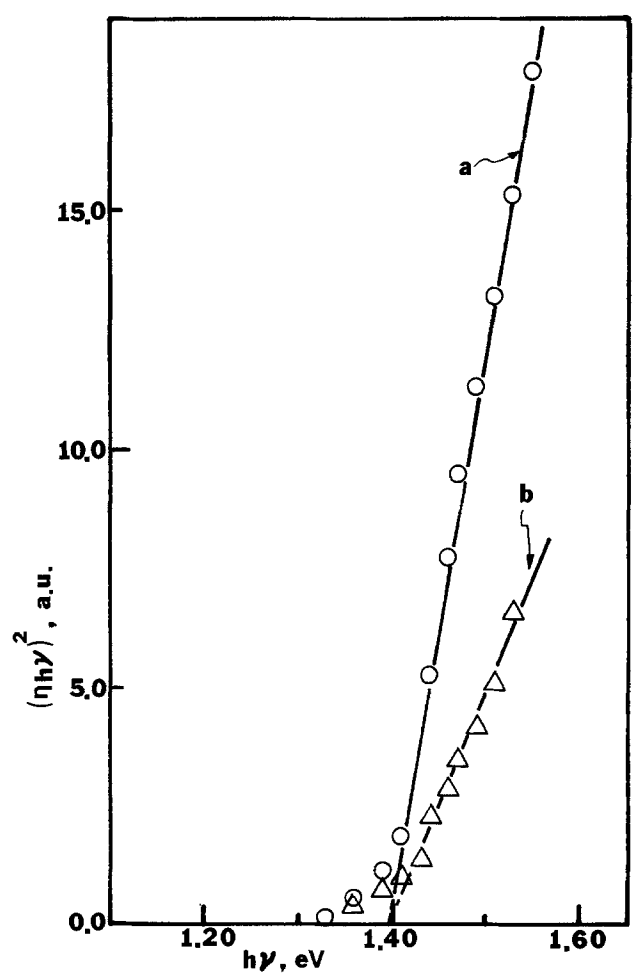

Fig. 9a. $(\eta h\nu)^2$ *vs.* $h\nu$ in aqueous solution containing 0.5M Na_2SO_4, 1.0M NaI, and 0.05M iodine. Here η is the quantum efficiency and $h\nu$ is the photon energy. (a) n-$MoSe_2$; (b) n-WSe_2. Electrodes are biased at 0.2V *vs.* SCE.

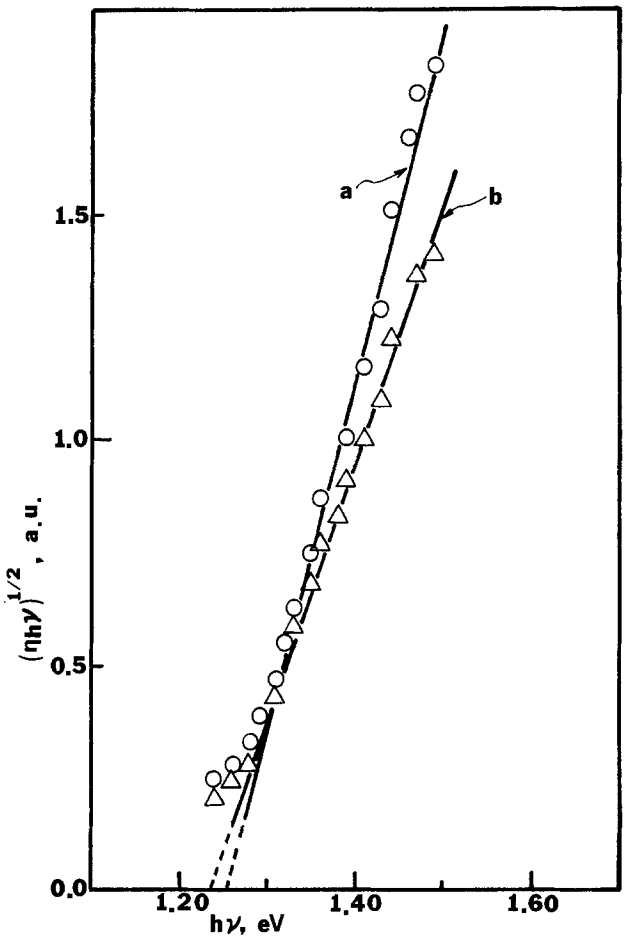

Fig. 9b. $(\eta h\nu)^{1/2}$ *vs.* $h\nu$ for (a) n-$MoSe_2$; (b) n-WSe_2. Same conditions as in Fig. 9a.

Br_2 solution. The light intensity dependence of the short-circuit photocurrent and the open-circuit photovoltage is shown in Fig. 12.

Discussion

The (n-$MoSe_2$/solution) interface.—A model for the behavior of the n-WSe_2/solution interface in aqueous electrolyte has been discussed previously (4). A similar model, *i.e.*, the recombinative model, is applicable to explain the voltammetric behavior of n-$MoSe_2$ in various redox electrolytes. V_{FB} of the n-$MoSe_2$ electrode determined from the impedance measurement is ~0.0V *vs.* SCE. When no specific adsorption occurs, the expected most negative V_{on} value was obtained for redox couples with $0 \leq V^o \leq 0.5$V *vs.* SCE. (The I^-/I_3^- couple involves adsorption effects and is discussed later.) For redox couples with V^o more positive than 0.5V, however, V_{on} occurs at more positive potentials. This can be ascribed to the effects of dark reduction of the oxidized form of redox couples. Recall that considerable dark reduction of the $Fe(CN)_6^{3-}$ takes place at a potential ~0.3V positive of V_{FB} (Fig. 7). The reduction of I_3^- occurred at more negative potentials probably because the bandedges shift with specific adsorption as suggested by the impedance measurements and the voltammetric experiments. For the couples with V^o more positive than 0.5V *vs.* SCE, *e.g.*, Fe^{2+}/Fe^{3+} and Br^-/Br_2, the reduction occurred at a potential ~0.5V *vs.* SCE. This positive shift of the zero current or onset potential might involve induced positive surface charges. The positive shift of V_{on} is attributed to the dark reduction of photogenerated species. There are several different mechanisms by which such dark reduction can occur at an n-type material at potentials significantly positive of that for V_{FB} (*i.e.*, of the energy of the conduction bandedge) in the supporting electro-

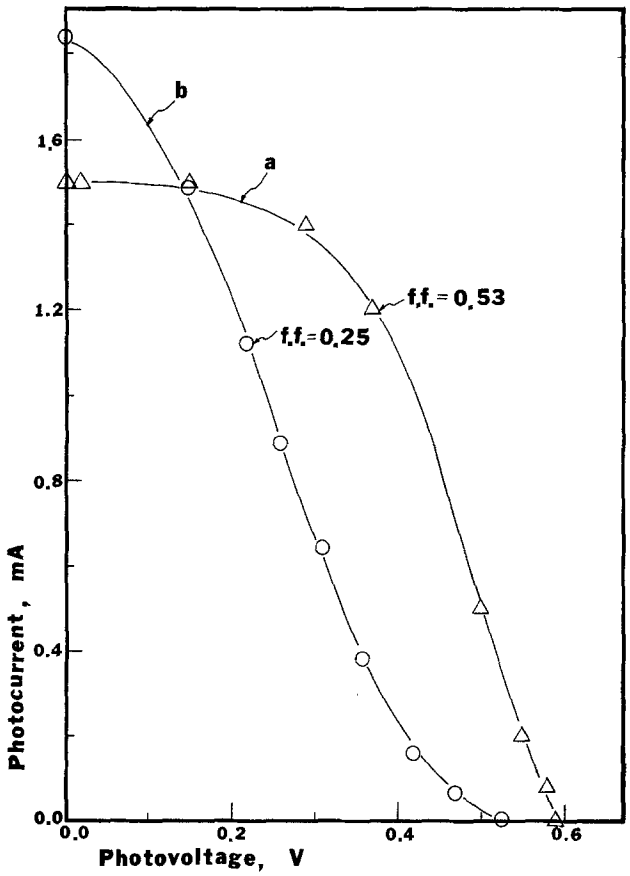

Fig. 10. Performance characteristics of n-$MoSe_2$ based PEC cells. 450W Xe lamp fitted with a 590 nm cut-on filter was used as the light source. (a) n-$MoSe_2$/0.50M Na_2SO_4, 0.50M H_2SO_4, 1.0M NaI, 0.05M I/Pt. (b) n-$MoSe_2$/0.50M Na_2SO_4, 0.50M H_2SO_4, 1.0M NaBr, 0.02M Br/Pt.

lyte solution. One involves a recombination model and the existence of filled surface states or intermediate levels at energies within the bandgap which can be emptied by electron donation to solution oxidants (or by photogenerated holes in the valence band) (16). The lack of detection of such states in the capacitance plots and the lack of significant dark anodic current implies that such states are very "slow" with respect to emptying via the conduction band. An alternative mechanism involves positive charge injection into the surface states (via solution species or photogenerated holes) causing a shift in the conduction bandedge toward more positive potentials and allowing electron transfer directly from the conduction band. This latter mechanism should result in a shift in V_{FB} in the presence of the redox couple; determination of such a shift by capacitance measurements are made difficult by the interference of faradaic reactions in determination of the actual space charge capacitance. Inversion could also cause such a shift in the bandedge (8); however, the location of the Fe^{3+}/Fe^{2+} couple is such that inversion would not occur at these potentials. A schematic representation of the energetic situation at the n-$MoSe_2$/solution interface, neglecting any band bending and specific surface interactions, is shown in Fig. 13. A direct-transition bandgap of 1.4 eV[6] is taken here based on the agreement of E_g determined from the action spectrum and the capacitance measurements for WSe_2 electrodes, discussed later.

Photovoltaic cells based on n-$MoSe_2$ electrodes.—The n-$MoSe_2/I^-$, I_3^-/Pt system shows a V_{oc} of 0.59V which is identical to the value predicted either from the experimental, ΔV, or the theoretical, $\Delta V'$, underpotential 0.59V, as shown in Table II. For the n-$MoSe_2/Br^-$,

[6] An indirect transition bandgap of 1.1 eV has been reported (8c). An E_g of 1.4 eV has also been reported (7).

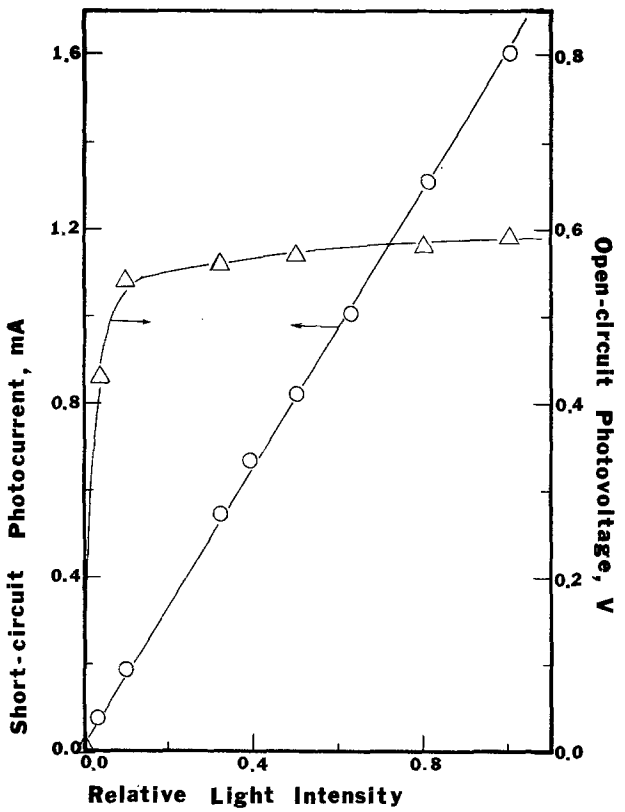

Fig. 11. Open-circuit photovoltage and short-circuit photocurrent as functions of light intensity. Same light source as in Fig. 10. Same solar cell as used in Fig. 10(a).

Br_2/Pt system, the V_{oc} of 0.52V was close to ΔV, 0.57V; however, it was much smaller than $\Delta V'$, 0.82V. This

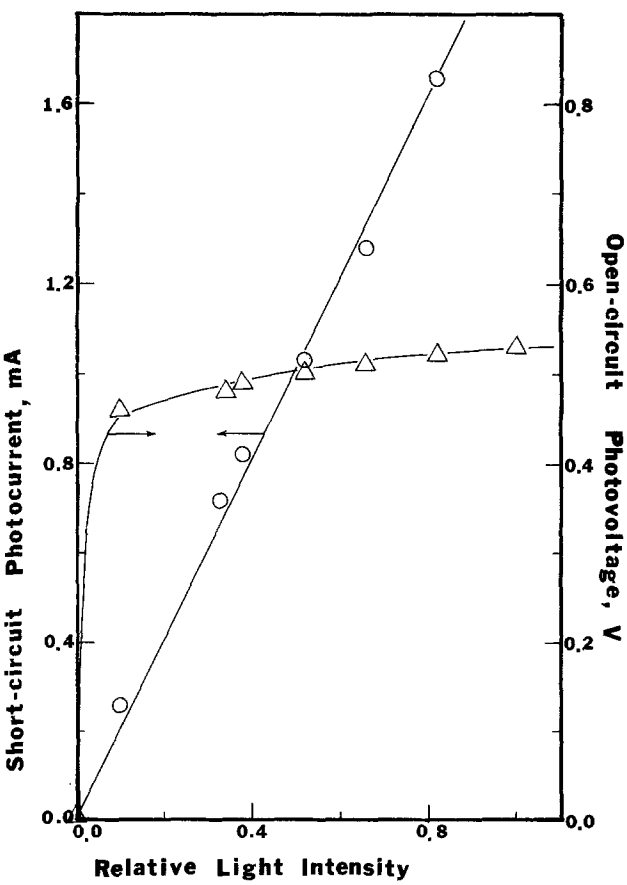

Fig. 12. Open-circuit photovoltage and short-circuit photocurrent as functions of light intensity. Same light source and solar cell as used in Fig. 10(b).

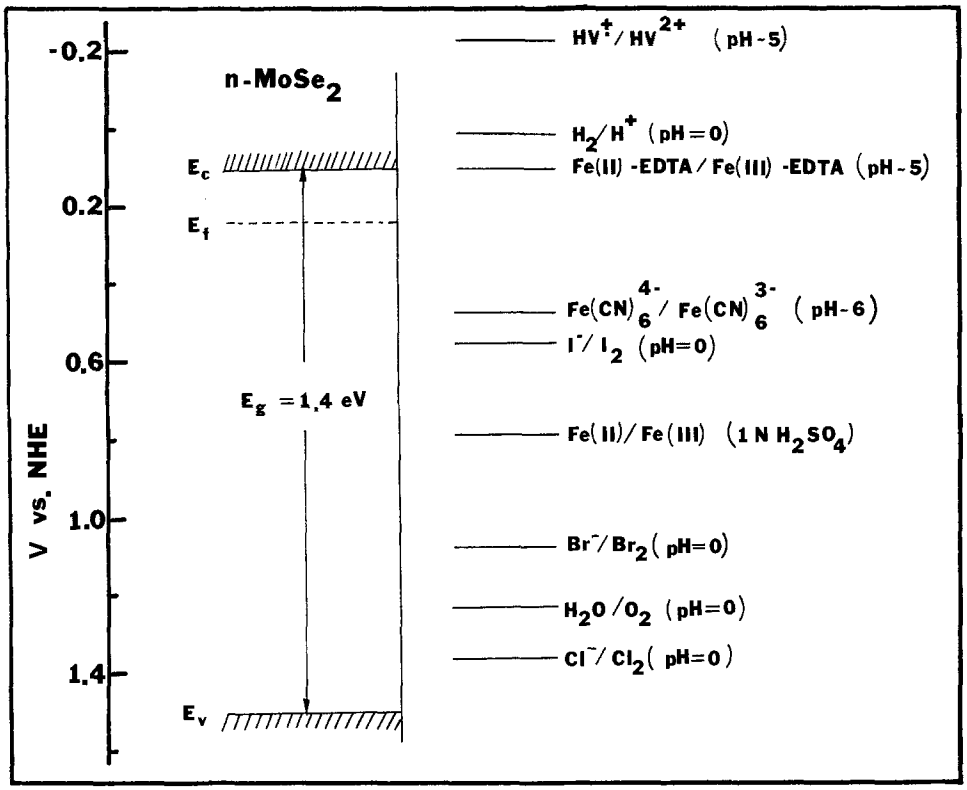

Fig. 13. Schematic representation of the energetic situation at the n-$MoSe_2$/solution interface. E_c = conduction bandedge; E_f = Fermi energy corresponding to flatband potential; E_v = valence bandedge; E_g = bandgap.

discrepancy can be attributed to the dark reduction processes or to a shift in the bandedges toward positive potentials because of induced positive surface charges. Besides this striking difference in V_{oc} between I^-/I_3^- and Br^-/Br_2 system, the fill factors for these two systems were also quite different, probably again because of the effects discussed above.

E_g of WSe_2.—As shown in Table I, E_v and E_c of WSe_2 in aqueous solution correspond to 0.93V and −0.44V *vs.* SCE, respectively. The uncertainty of E_v and E_c due to the uncertainties in the dielectric constant taken here is less than 20 meV. Thus E_g of WSe_2 is $\sim$ (1.4 $\pm$ 0.05) eV. This agrees fairly well with the direct transition bandgap determined from the action spectrum of the photocurrent.

Acknowledgment

This work was supported by a grant from the Solar Energy Research Institute. We are grateful to Dr. Miller and Dr. DiSalvo for providing the samples of the semiconductor materials.

Manuscript submitted Oct. 17, 1980; revised manuscript received Dec. 29, 1980.

Any discussion of this paper will appear in a Discussion Section to be published in the December 1981 JOURNAL. All discussions for the December 1981 Discussion Section should be submitted by Aug. 1, 1981.

Publication costs of this article were assisted by the University of Texas.

REFERENCES

1. (a) A. J. Bard, *J. Photochem.*, **10,** 59 (1979); (b) A. J. Bard, *Science,* **207,** 139 (1980); (c) M. S. Wrighton, *Acc. Chem. Res.*, **12,** 303 (1979); (d) A. J. Nozik, *Ann. Rev. Phys. Chem.*, **29,** 189 (1978).
2. (a) H. Tributsch and J. C. Bennett, *J. Electroanal. Chem. Interfacial Electrochem.*, **81,** 97 (1977); (b) H. Tributsch, *Ber. Bunsenges. Phys. Chem.*, **81,** 361 (1977); (c) H. Tributsch, *ibid.*, **82,** 169 (1978); (d) H. Tributsch, *This Journal,* **125,** 1086 (1978); (e) J. Gobrecht, H. Gerischer, and H. Tributsch, *ibid.*, **125,** 2085 (1978); (f) L. F. Schneemeyer and M. S. Wrighton, *J. Am. Chem. Soc.*, **101,** 6496 (1979); (g) L. F. Schneemeyer, M. S. Wrighton, A. Stacy, and M. J. Sienko, *Appl. Phys. Lett.*, **36,** 701 (1980); (h) J. Gobrecht, H. Gerischer, and H. Tributsch, *Ber. Bunsenges. Phys. Chem.*, **82,** 1331 (1978); (i) H. Tributsch, H. Gerischer, C. Clemen, and E. Bucher, *ibid.*, **83,** 655 (1979).
3. C. P. Kubiak, L. F. Schneemeyer, and M. S. Wrighton, *J. Am. Chem. Soc.*, In press.
4. (a) F-R. F. Fan, H. S. White, B. Wheeler, and A. J. Bard, *J. Am. Chem. Soc.*, **102,** 5142 (1980); (b) F-R. F. Fan, H. S. White, B. Wheeler, and A. J. Bard, *This Journal,* **127,** 518 (1980); (c) H. S. White, F-R. F. Fan, and A. J. Bard, *ibid.*, 128, 1045 (1981).
5. B. A. Parkinson, T. E. Furtak, and D. Canfield, Paper No. 23 in *Faraday Society Discussion, No. 70,* The Royal Society of Chemistry, London (September 1980).
6. H. J. Lewerenz, A. Heller, and F. J. DiSalvo, *J. Am. Chem. Soc.*, **102,** 1877 (1980).
7. S. Menezes, F. J. DiSalvo, and B. J. Miller, *This Journal,* In press.
8. (a) W. Kautek, H. Gerischer, and H. Tributsch, *Ber. Bunsenges. Phys. Chem.*, **83,** 1000 (1979); (b) S. M. Ahmed and H. Gerischer, *Electrochim. Acta.*, **24,** 705 (1979); (c) W. Kautek and H. Gerischer, *This Journal,* **127,** 2471 (1980).
9. V. A. Myamlin and Yu. V. Pleskov, "Electrochemistry of Semiconductors," Plenum Press, New York (1967).
10. B. L. Evans and P. A. Young, *Proc. R. Soc. London, Ser. A,* **284,** 402 (1965); see also A. R. Beal and H. P. Hughs, *J. Phys. C,* **12,** 881 (1979).
11. W. T. Hicks, *This Journal,* **111,** 1058 (1964).
12. J. A. Wilson and A. D. Yoffe, *Adv. Phys.*, **18,** 193 (1969).
13. A. R. Beal, W. Y. Liang, and H. P. Hughs, *J. Phys. C,* **9,** 2449 (1976).
14. (a) M. A. Butler, *J. Appl. Phys.*, **48,** 1914 (1977); (b) J. J. Earnest, in "Semiconductors and Semimetals," Vol. 3, R. K. Willardson and Albert C. Beer, Editors, Chap. 6, Academic Press, New York (1967).
15. P. G. P. Ang and A. F. Sammells, Paper No. 11 in *Faraday Society Discussion, No. 70,* The Royal Society of Chemistry, London (September 1980).
16. S. N. Frank and A. J. Bard, *J. Am. Chem. Soc.*, **97,** 7427 (1975).